

Atomistic Measures of Materials Strength and Deformation

Ju Li, Wei Cai, Jinpeng Chang, Sidney Yip

Department of Nuclear Engineering

Massachusetts Institute of Technology, Cambridge, MA 02139 USA

Abstract. Multiscale materials modeling has emerged as a significant concept as well as a unique approach in computational materials research. We examine here the role of atomistic simulations in modeling the structural responses of solids to thermal and mechanical loading, particularly with regard to the mechanistic understanding derived from the atomic-level details generally not available from experiments. Theoretical strength is defined through elastic modes of instability, or more generally, through the onset of soft vibrational modes in the deformed lattice. Molecular dynamics (MD) simulation of stress-strain response provides a direct measure of the effects of small-scale microstructure on strength, as illustrated by results on single crystal, amorphous, and nanocrystalline phases. In the kinetics of melting, we distinguish between the thermoelastic process of mechanical melting which is homogeneous and sets the upper of metastability of the lattice, and the free-energy driven process of thermodynamics melting which involves nucleation and growth and is therefore heterogeneous. In the kinetics of defect mobility we study dislocation dynamics by direct MD simulation and a mesoscale (kinetic Monte Carlo) which couples kink mechanism energetics to the experimentally measured dislocation velocity. In the area of crack propagation, the fundamental problems of brittle-ductile transition and crack-tip plasticity are two well-known problems in fracture mechanics that have been looked at from the atomistic standpoint. From these case studies one may gain some appreciation of the capabilities, as well limitations, of atomistic simulations to provide physical insight in computational materials research.

1. Introduction

Understanding materials behavior at the atomic level has long been a grand challenge to scientists and engineers across many disciplines. Currently there is widespread interest in identifying fundamental problems in materials modeling which combine scientific challenges with technologically relevant applications [1]. To provide a basis for such inquiries, we discuss here a particular focus on the molecular understanding of mechanical behavior, in the context of a multiscale approach to materials theory and simulation [2,3]. The aim of this chapter, written in the spirit of a set of lecture notes, is to discuss how strength and deformation at the atomistic level can be probed through structural instability and modes of dynamical response to critical loading, through heating

or an applied stress. In examining several case studies we hope the readers will feel stimulated to draw analogies between fundamental issues which sometimes are considered only separately, such as thermal versus mechanical responses, elastic and plastic deformations, and homogenous and heterogeneous processes. By noting the contrasts and parallels between the individual topics discussed, we believe it is possible to appreciate the role of atomistic simulations in probing complex systems phenomena in the materials research arena and beyond.

2. Limits to Strength: Structural Instabilities

The theoretical basis for describing the mechanical stability of a crystal lattice lies in the formulation of stability conditions which specify the critical level of external stress that the system can withstand. Lattice stability is not only one of the most central issues in elasticity, it is also fundamental in any analysis of structural transitions in solids, such as polymorphism, amorphization, fracture, or melting. In these notes our goal is to discuss the role of elastic stability criteria at finite strain in elucidating the competing mechanisms underlying a variety of structural instabilities, and the physical insights that may be gained by probing stress and temperature induced structural responses through atomistic simulations.

Born has shown that by expanding the internal energy of a crystal in a power series in the strain and requiring positivity of the energy, one obtains a set of conditions on the elastic constants of the crystal that must be satisfied to maintain structural stability of the lattice [4,5]. This then leads to the determination of ideal strength of perfect crystals as an instability phenomenon, a concept which has been examined by Hill [6] and Hill and Milstein [7], as well as used in various applications [8]. That Born's results are valid only when the solid is under zero external stress has been explicitly pointed out in a later derivation by Wang et al [9] invoking the formulation of a Gibbs integral. Further discussions were given by Zhou and Joos [10] and by Morris and Krenn [11], the latter emphasizing the thermodynamic basis of the concept of theoretical strength by showing that the conditions of elastic stability, based on Gibbs' original formulation [12], are identical to the results of Wang et al. in which the loading mechanism fixes the Cauchy stress. A consequence of these investigations is that theoretical strength should be considered a property which can be affected by the symmetry and magnitude of the applied load, rather than an intrinsic property of the material system only. In this respect the study of theoretical limits to material strength using atomistic models, including first-principles calculations [13], promises to yield new insights into mechanisms of structural instability.

While the stability criteria say nothing about the final state toward which a structurally unstable system will evolve, nevertheless they can be invaluable in interpreting molecular dynamics simulation results. In the context of simulating the outcome of a virtual strength test, quantitative predictions can be made of the maximum deformation (strain) the lattice can sustain, and the competition between different modes of instability can be analyzed. In this section we will first give a brief derivation of elastic stability at finite strain to bring out in a direct manner the interplay between the intrinsic response to deformation and the effect of external work. Then we note that vibrational instability in the form of soft phonon modes is an extension of this concept, and that direct molecular dynamics simulation can be used to probe both. In the last part of this section we consider briefly the how strength is affected by the microstructure of the material. Since a crystal attains its ideal (maximum) strength in the absence of any defect, it is that the presence of any microstructural features, such as disorder or interfaces, will lower the strength.

2.1 Elastic Stability Criteria

Consider a perfect lattice undergoing homogeneous deformation under an applied stress τ , where the system configuration changes from X to $Y = JX$, with J being the deformation gradient or the Jacobian matrix. The associated Lagrangian strain tensor is

$$\eta = (1/2)(J^T J - 1) \quad (1)$$

Let the change in the Helmholtz free energy be expressed by an expansion in η to second order,

$$\begin{aligned} \Delta F &= F(X, \eta) - F(X, 0) \\ &= V(X)[t(X)\eta + (1/2)C(X)\eta\eta] \end{aligned} \quad (2)$$

where V is the volume, t the conjugate stress which is also known as the thermodynamic tension or the second (symmetric) Piola-Kirchhoff stress, and C the fourth-order elastic constant tensor. For the work done by an applied stress τ , which is commonly called the Cauchy or true stress, we imagine a virtual move near Y along a path where $J \rightarrow J + \delta J$ which results in an incremental work

$$\begin{aligned} \delta W &= \oint_S \tau_{ij} n_j \delta u_i dS \\ &= V(Y) \frac{\tau_{ij}}{2} \left(\frac{\partial u_i}{\partial Y_j} + \frac{\partial u_j}{\partial Y_i} \right) \\ &= V(Y) \text{Tr}(J^{-1} \tau J^T \delta \eta) \end{aligned} \quad (3)$$

The work done over a deformation path ℓ , $\Delta W(\ell)$, is the integral of δW , given by Eq.(3), over the path. To examine the lattice stability at configuration X , we now consider the difference between the increase in Helmholtz free energy and the work done by the external stress,

$$\begin{aligned} \Delta G(Y, \ell) &= \Delta F(X, \eta) - \Delta W(\ell) \\ &= \int_{\ell} g(Y) d\eta \end{aligned} \quad (4)$$

where

$$g(Y) = \frac{\partial F}{\partial \eta} - V(Y) J^{-1} \tau J^T \quad (5)$$

One may also interpret ΔG in the spirit of a virtual work argument. If the work done by the applied stress exceeds that which is absorbed as the free energy increase, then an excess amount of energy would be available to cause the displacement to increase and the lattice would become unstable.

We regard ΔG as a Gibbs integral in analogy with the Gibbs free energy, the appropriate thermodynamic potential in the (NTP) ensemble. However, notice that ΔG is in general dependent on the deformation path through the external work contribution. This means that strictly speaking it is not a true thermodynamic potential on which one can perform the usual stability analysis. Nevertheless, $-g(Y)$ can be treated as a force field in

deformation space for the purpose of carrying out a stability analysis [9]. Suppose the lattice, initially at equilibrium at X under stress τ , is perturbed to configuration Y with corresponding strain η . A first-order expansion of $g(Y)$ gives

$$g_{ij}(\eta) = V(Y)B_{ijkl}\eta_{kl} + \dots \quad (6)$$

where, by using $V(Y) = V(X)\det|J|$, one obtains

$$\begin{aligned} B_{ijkl} &= C_{ijkl} - \left[\frac{\partial(\det|J|J_{im}^{-1}\tau_{mn}J_{nj}^{-1})}{\partial\eta_{kl}} \right]_{\eta=0, J=I} \\ &= C_{ijkl} + \Lambda_{ijkl}(\tau) \end{aligned} \quad (7)$$

with

$$\Lambda_{ijkl}(\tau) = (1/2)[\delta_{ik}\tau_{jl} + \delta_{jk}\tau_{il} + \delta_{il}\tau_{jk} + \delta_{jl}\tau_{ik} - 2\delta_{kl}\tau_{ij}] \quad (8)$$

δ_{ij} being the Kronecker delta symbol for indices i and j. The physical implication of Eq.(6) is that in deformation space the shape of the force field around the origin is described by B. The stability condition is then the requirement that all the eigenvalues of B be positive, or

$$\det|A| > 0 \quad (9)$$

where $A = (1/2)(B^T + B)$, with B being in general asymmetric [9]. In cases where the deformation gradient J is constrained to be symmetric, as in certain atomistic simulations at constant stress, one can argue that the condition $\det|B| > 0$ is quite robust [9]. Thus, lattice stability is governed by the fourth-rank tensor B, a quantity which has been called the elastic stiffness coefficient [14]. It differs from the conventional elastic constant by the tensor Λ which is a linear function of the applied stress. The foregoing derivation shows clearly the effect of external work which was not taken into account in Born's treatment. In the limit of vanishing applied stress one recovers the stability criteria given by Born [4,5].

In the present discussion we will consider only cubic lattices under hydrostatic loading in which case the stability criteria take on a particularly simple form,

$$\begin{aligned} K &= (1/3)(C_{11} + 2C_{12} + P) > 0 \\ G' &= (1/2)(C_{11} - C_{12} - 2P) > 0 \\ G &= C_{44} - P > 0 \end{aligned} \quad (10)$$

where C_{ij} are the elastic constants at current pressure P, $P > 0$ (< 0) for compression (tension). K is seen to be the isothermal bulk modulus, G' and G the tetragonal and rhombohedral shear moduli respectively. The theoretical strength is that value of P for which one of the three conditions in Eq.(10) is first violated. A simple demonstration showing that the external load must appear in the stability criteria is to subject a crystal to hydrostatic tension by direct atomistic simulation using a reasonable interatomic potential. In this case one finds the instability mode is the vanishing of K, whereas the Born criteria, Eq.(10) with P set equal to zero, would predict the vanishing of G' [9].

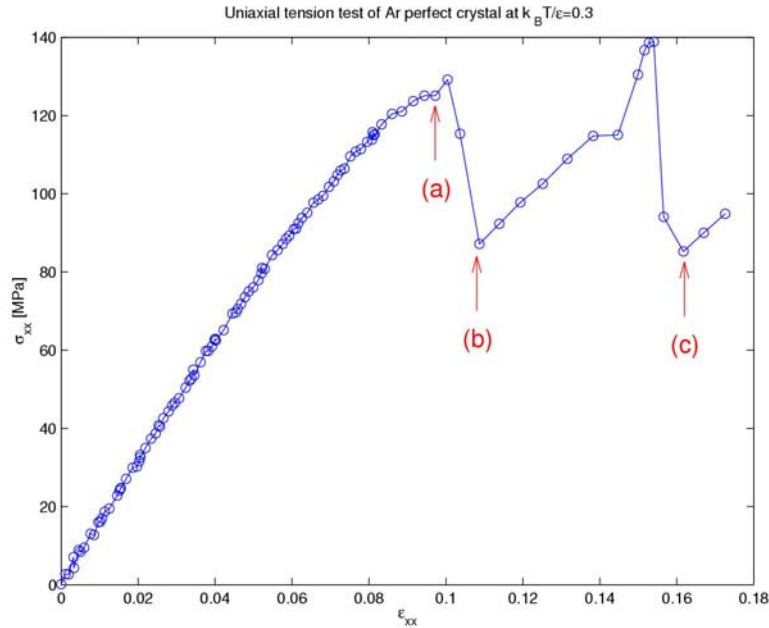
It is worth mentioning that the six components of the eigenmodes of deformation corresponding to the three zero eigenvalues of $\det(B)$ are $(1,1,1,0,0,0)\delta\eta$, $(\delta\eta_{xx}, \delta\eta_{yy}, \delta\eta_{zz}, \mathbf{0}, \mathbf{0}, \mathbf{0})$ with $\delta\eta_{xx} + \delta\eta_{yy} + \delta\eta_{zz} = \mathbf{0}$ in the order indicated in Eq.(10) [9]. The deformation when the bulk modulus vanishes (spinodal instability) preserves the cubic symmetry, while for the tetragonal shear instability the cubic symmetry must be broken.

The connection between stability criteria and theoretical strength is rather straightforward. For a given applied stress $\underline{\sigma}$ one can imagine evaluating the current elastic constants to obtain the stiffness coefficients B . Then by increasing the magnitude of $\underline{\sigma}$ one will reach a point where one of the eigenvalues of the matrix A (cf. Eq.(3)) vanishes. This critical stress at which the system becomes structurally unstable is then a measure of theoretical strength of the solid. In view of this, one has a direct approach to strength determination through atomistic simulation of the structural instability under a prescribed loading. If the simulation is performed by molecular dynamics, temperature effects can be taken into account naturally by following the particle trajectories at the temperature of interest.

Under a uniform load the deformation of a single crystal is homogeneous up to the point of structural instability. For a cubic lattice under an applied hydrostatic stress, the load-dependent stability conditions are particularly simple, being of the form

$$B = (C_{11} + 2C_{12} + P) / 3 > 0, \quad G' = (C_{11} - C_{12} - 2P) / 2 > 0, \quad G = C_{44} - P > 0 \quad (11)$$

where P is positive (negative) for compression (tension), and the elastic constants C_{ij} are to be evaluated at the current state. While this result is known for some time [15-17], direct verification against atomistic simulations showing that the criteria do accurately describe the critical value of P (P_c) at which the homogeneous lattice becomes unstable has been relatively recent [9, 18-22]. One may therefore regard P_c as a definition of theoretical or ideal tensile (compressive) strength of the lattice.



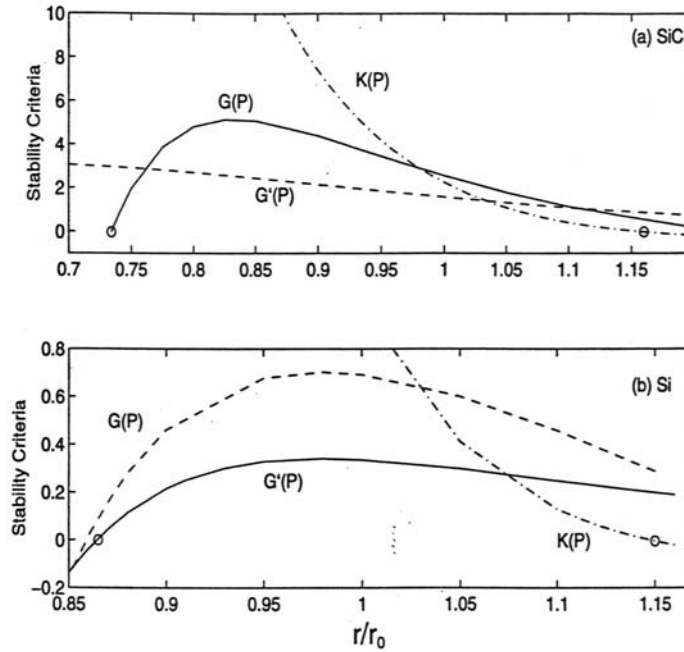


Fig.1. Variation of elastic moduli, K , G , and G' , with lattice strain under hydrostatic loading at 0 K, (a) β -SiC, and (b) Si. $r/r_0 = 1$ denotes the condition of zero stress.

Turning now to molecular dynamics simulations we show in Fig. 1 the stress-strain response for a single crystal of Ar under uniaxial tension at 35.9K. At every step of fixed strain, the system is relaxed and the virial stress evaluated. One sees the expected linear elastic response at small strain up to about 0.05; thereafter the response is nonlinear but still elastic up to a critical strain of 0.1 and corresponding stress of 130 MPa. Applying a small increment strain beyond this point causes a dramatic stress reduction (relief) at point (b). Inspection of the atomic configurations at the indicated points shows the following. At point (a) several point defect like inhomogeneities have been formed; most probably one or more will act as nucleation sites for a larger defect which causes the strain energy to be abruptly released. At the cusp, point (b), one can clearly discern an elementary slip on an entire [111] plane, the process being so sudden that it is difficult to capture the intermediate configurations. Figuratively speaking, we suspect that a dislocation loop is spontaneously created on the (111) plane which expands at a high speed to join with other loops or inhomogeneities until it annihilates with itself on the opposite side of the periodic border of the simulation cell, leaving a stacking fault. As one increases the strain the lattice loads up again until another slip occurs. At (c) one finds that a different slip system is activated.

2.2 Soft Modes

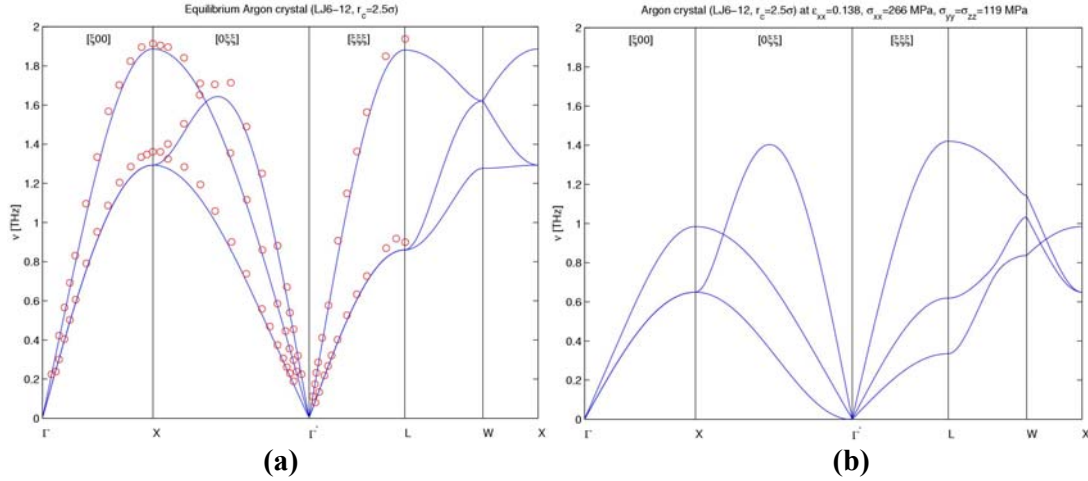


Fig. 2. Phonon dispersion curves of single crystal of Ar as described by the Lennard-Jones potential (solid lines), (a) comparison of results for equilibrium condition with experimental data (circles), (b) results for uniaxial tension deformation at strain of 0.138 (corresponding stresses of 266 MPa and 119 MPa along the tensile and transverse direction).

One may regard the stability criteria, Eq.(5), as manifestation in the long wavelength limit of the general condition for vibrational stability of a lattice. The vanishing of elastic constants then corresponds to the phenomenon of soft phonon modes in lattice dynamics. Indeed one finds that under sufficient deformation such soft modes do occur in a homogeneously strained lattice. To see the lattice dynamical manifestation of this condition, we apply molecular dynamics to relax a single crystal sample with periodic boundary condition at essentially zero temperature for a specified deformation at constant strain. The resulting atomic configurations are then used to construct and diagonalize the dynamical matrix. Fig. 2 shows two sets of dispersion curves for the Lennard-Jones interatomic potential describing Ar which has fcc structure, one for the crystal at equilibrium (for reference) and the other when the lattice is deformed under a uniaxial tensile strain of 0.138 which is close to the critical value [23]. One can see in the latter a Γ' -point soft mode in the [011] direction. Similar results for deformation under shear or hydrostatic tensile strain would show soft modes Γ' -point in the [111] direction and Γ -point in the [100] direction respectively. All these are acoustic zone-center modes, therefore they would correspond to elastic instabilities. For a more complicated lattice such as SiC in the zinc blende structure, one would find that soft modes also can occur at the zone center [23]. The overall implication here is that lattice vibrational analysis of a deformed crystal offers the most general measure of structural instability, and this again demonstrates that strength is not an intrinsic property of the material, rather it depends on the mode of deformation.

2.3 Microstructural Effects

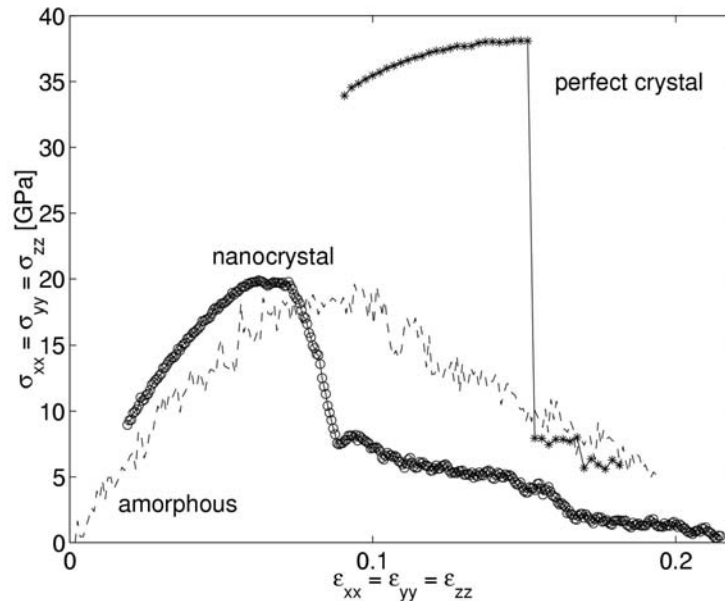


Fig. 1 is a typical stress-strain response on which one can conduct very detailed analysis of the deformation using the atomic configuration available from the simulation. This atomic-level version of structure-property correlation can be even more insightful than the conventional macroscopic counterpart simply because in simulation the microstructure can be as well characterized as one desires. As an illustration we repeat the deformation simulation using as initial structures other atomic configurations which have some distinctive microstructural features. We have performed such studies on cubic SiC (3C or beta phase) which has zinc-blends structure, using an empirical bond-order potential [24] and comparing the results for a single crystal and prepared amorphous and nanocrystalline structures.[23] Fig. 3 shows the stress-strain response for under hydrostatic tension at 300K. At every step of fixed strain, the system is relaxed and the virial stress evaluated. Three samples are studied, all with periodic boundary conditions, a single crystal (3C), an amorphous system that is an enlargement of a smaller configuration produced by electronic-structure calculations [25], and a nanocrystal composed of four distinct grains with random orientations (7810 atoms). As in Fig. 1, the single-crystal sample shows the expected linear elastic response at small strain up to about 0.03; thereafter the response is nonlinear but still elastic up to a critical strain of 0.155 and corresponding stress of 38 GPa. Applying a small increment strain beyond this point causes a dramatic change with the internal stress suddenly reduced by a factor of 4. Inspection of the atomic configurations (not shown) reveals the nucleation of an elliptical microcrack in the lattice along the direction of maximum tension. With further strain increments the specimen deforms by strain localization around the crack with essentially no change in the system stress.

The responses of the amorphous and nanocrystal SiC differ significantly from that of the single crystal. The former shows a broad peak, at about half the critical strain and stress, suggesting a much more gradual structural transition. Indeed, the deformed atomic configuration reveals channel-like decohesion at strain of 0.096 and stress 22 GPa. Another feature of the amorphous sample is that the response to other modes of deformation, uniaxial tension and shear, is much more isotropic relative to the single crystal, which is perhaps understandable with bonding in SiC being quite strongly covalent and therefore directionally dependent. For the nanocrystal, the critical strain and stress are similar to the amorphous phase, except that the instability effect is much more pronounced, qualitatively like that of the single crystal. The atomic configuration shows rather clearly the failure process to be intergranular decohesion. These observations allow us to correlate the qualitative behavior of the stress-strain responses with a gross feature of the system

microstructure, namely, the local disorder (or free volume). This feature is of course completely absent in the single crystal, well distributed in the amorphous phase, and localized at the grain boundaries in the nanocrystal. The disorder can act as a nucleation site for structural instability, thereby causing a reduction of the critical stress and strain for failure. Once a site is activated, it will tend to link up with neighboring activated sites, thus giving rise to different behavior between the amorphous and nanocrystal samples.

3. Mechanistic Aspects (Kinetics) of Melting

In 1939 Born set forth a simple criterion for crystal melting by postulating that melting should be accompanied by the loss of shear rigidity.[26] Expressed in terms of the shear modulus G for a cubic crystal, the melting point T_m is that temperature at which

$$G(T_m) = 0 \quad (12)$$

A year later he extended this stability concept to lattice deformation [4] by deriving the conditions for mechanical stability which in the case of cubic crystals are given by

$$C_{11} + 2C_{12} > 0, \quad C_{11} - C_{12} > 0, \quad C_{44} > 0 \quad (13)$$

These can be obtained from stability criteria, (11), derived in Sec. 2.1 under the condition of no external stress. In this section we will examine the basis on which Born's two criteria may be considered to be valid. Shortly after (12) was proposed, experimental results obtained on NaCl single crystals were presented showing that the two shear constants, C_{44} and $(C_{11} - C_{12})$, have nonzero values at the melting point.[27] Moreover, it was not clear how this criterion could explain the existence of latent heat and volume change in a first-order thermodynamic phase transition. In contrast, the stability criteria (13) seem to be generally accepted, with neither stringent tests having been performed nor qualifications concerning its possible limitations discussed. The challenge of ascertaining whether such criteria are capable of predicting the actual onset of an instability is considerable. The difficulty, on the theoretical side, has been that stability analyses have been formulated in different ways [6,7], and few explicit calculations of elastic constants at the critical condition have been reported to make possible an unambiguous test. On the experimental side, competing effects frequently render the determination of the triggering instability uncertain. Thus, while the shortcomings of (12) are well known, the use of (13) to define structural resistance to thermal agitation has gone unnoticed.

3.1 Mechanical Melting – Limit of Metastability

Our interest here is to test (13) through molecular dynamics simulation of melting instead of testing (12) using experimental data. By performing simulation of isobaric heating to melting at zero pressure of a perfect crystal without surfaces or defects of any kind, we achieve an unambiguous test since without an external stress (13) would be equivalent to (11). As we will see below, simulation shows that at the onset of melting one of the shear constants indeed vanishes, although it is $(C_{11} - C_{12})$ rather than C_{44} . The observed melting temperature, or equivalently the critical lattice strain, is in remarkable agreement with the predictions based on the stability criteria. Since the system is initially a defect- and surface-free lattice, the homogeneous melting observed here is to be distinguished from the conventional melting which is a free-energy based heterogeneous process of nucleation and growth. The latter process, if not kinetically suppressed in simulation by eliminating all defects and surfaces, would set in at a lower temperature, the

conventional melting point of the material, and preclude the melting process associated with an elastic instability. Allowing for these modifications, the melting and stability criteria proposed by Born are reconciled. The qualification which is nontrivial is that the concept of thermoelastic mechanism of melting indeed applies to a form of melting, but it is melting in the sense of mechanical stability against thermal excitation as opposed to the conventional thermodynamic process which is always defect mediated and therefore heterogeneous.

Given that the generalized criteria (11) obviously reduce to Born's results in the limit of zero load, then (13) is a valid description of lattice stability in the special case of a cubic crystal being heated to melting at zero pressure. For the simulation we use an interatomic potential model for Au [28] (details of the potential are of no interest in this discussion) and a simulation cell containing 1372 atoms with periodic border conditions imposed in the manner of Parrinello and Rahman.[29] A series of isobaric-isothermal simulations (with velocity rescaling) are carried out at various temperatures. At each temperature the atomic trajectories generated are used to compute the elastic constants at the current state using appropriate fluctuation formulas.[30]

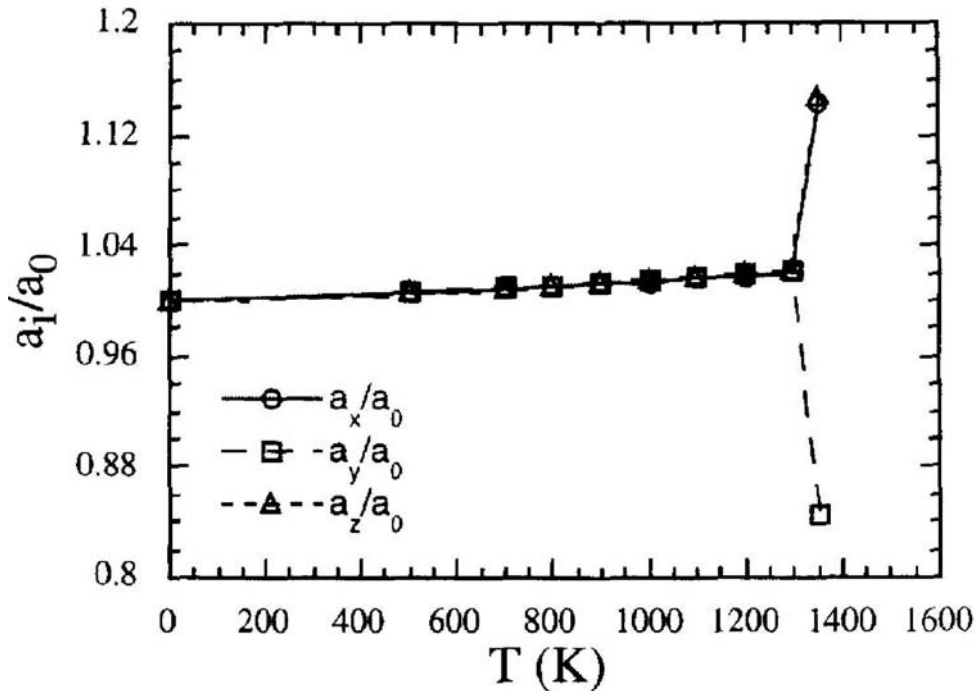


Fig. 4 shows the variation with temperature of the lattice strain a/a_0 along the three cubic symmetry directions.[31] The slight increase with increasing temperature merely indicates the lattice is expanding normally with temperature, and the results for the three directions are the same as they should be. At $T = 1350$ K one sees a sharp bifurcation in the lattice dimension where the system elongates in two directions and contracts in the third. This is a clear sign of symmetry change, in the present case from cubic to tetragonal. To see whether the simulation results are in agreement with the prediction based on (7), we show in Fig. 5 the variation of the elastic moduli with temperature, or equivalently the lattice strain since there is a one-to-one correspondence as indicated in Fig. 3; the three moduli of interest are the bulk modulus $B_T = (C_{11} + 2C_{12})/3$, tetragonal shear modulus $G' = (C_{11} - C_{12})/2$, and rhombohedral shear modulus $G = C_{44}$. On the basis of Fig. 4 one would predict the incipient instability to be the vanishing of G' , occurring at the theoretical or predicted lattice strain of $(a/a_0)_{th} = 1.025$. From the simulation at $T = 1350$ the observed

strain is $(a/a_0)_{\text{obs}} = 1.024$. Thus, we can conclude that the vanishing of tetragonal shear is responsible for the structural behavior.

For more details of the system behavior at $T = 1350$ K we show in Fig. 6 the time evolution of the lattice strain, the off-diagonal elements of the cell matrix H , and the system volume. It is clear from Fig. 6(a) that the onset of the $G' = 0$ instability triggers both a shear (cf. Fig. 6(b)) and a lattice decohesion (Fig. 6(c)), the latter providing the characteristic volume expansion associated with melting. This sequence of behavior, which has not been recognized previously, implies that the signature of a first-order transition, namely, latent volume change, is not necessarily associated with the incipient instability. Our results also provide evidence supporting Born's picture of melting being driven by a thermoelastic instability [26], later reinterpreted by Boyer [32] to involve a combination of loss of shear rigidity and vanishing of the compressibility. Moreover, it is essential to recognize that this thermoelastic mechanism can only be applied to the process of mechanical instability (homogeneous melting) of a crystal lattice without defects, and not to the coexistence of solid and liquid phases at a specific temperature (heterogeneous melting).[33,34]

It is perhaps worthwhile emphasizing again what the combination of stability analysis and molecular dynamics simulation has contributed to the understanding of Born's two criteria. That the stability criteria (13) are valid only under vanishing external load is quite clear, both theoretically and in simulation studies. Since it is often advantageous to be able to predict a priori the critical stress or strain for the onset of instability, the availability of (11) could facilitate more quantitative analysis of simulation results. Although our results for an fcc lattice with metallic interactions show that homogeneous melting is triggered by $G' = 0$ and not (6), nevertheless, they constitute clear-cut evidence that a shear instability is responsible for initiating the transition. The fact that simulation reveals a sequence of responses apparently linked to the competing modes of instabilities (cf. Fig. 6) implies that it is no longer necessary to explain all the known characteristic features of melting on the basis of the vanishing of a single modulus. In other words, independent of whether $G'=0$ is the initiating mechanism, the system will in any event undergo volume change and latent heat release in sufficiently rapid order (on the time scale of physical observation) that these processes are all identified as part of the melting phenomenon. Generalizing this observation further, one may entertain the notion of a hierarchy of interrelated stability catastrophes of different origins, elastic, thermodynamic, vibrational, and entropic.[35]

Finally it may be mentioned that in several studies over the last few years, the stability criteria (11) have led to precise identifications of the elastic instability triggering a particular structural transition. In hydrostatic compression of Si, the instability which causes the transition from diamond cubic to β -tin structure is the vanishing of $G'(P) = (C_{11} - C_{12} - 2P)/2$. [19] In contrast, compression of crystalline SiC in the zinc blende structure results in an amorphization transition associated with the vanishing of $G(P) = C_{44} - P$. [22] This is discussed further in the next section. For behavior under tension, crack nucleation in SiC [20] and cavitation in a model binary intermetallic [21], both triggered by the spinodal instability, vanishing of $B_T(P) = (C_{11} + 2C_{12} + P)/3$, are results which are analogous to the observations reported here. Notice also that in the present study a crossover from spinodal to shear instability can take place at sufficiently high temperature.[9]

3.2 Thermodynamic Melting

In the preceding simulations we encountered a melting transition which occurred in a perfect crystal that has no surfaces, because the MD simulation was carried out with

periodic boundary conditions. A critical temperature was reached at which a bifurcation took place with the cubic simulation cell suddenly becoming tetragonal, and the shear modulus G' vanished. The system responses triggered by this event, along with the atomic configurations, all show that the crystal has melted in a homogeneous manner; it may seem logical to thus conclude that the critical temperature is the melting point of the material. However, such an interpretation would prove to be hasty. We now show that when the heating-to-melting simulation is applied to a crystal with an initial defect such as a free surface or an interface, the crystal-to-liquid transition then occurs through a defect-nucleated process at a temperature *lower* than the critical temperature previously observed. Thus there exist two types of melting transitions, a heterogeneous process of nucleation and growth which corresponds to the conventional melting phenomenon, and a homogeneous process of mechanical collapse of the lattice. Henceforth we will refer to the two as *thermodynamic* and *mechanical* melting respectively, with corresponding melting points denoted as T_m and T_s . While the significance of the former needs no comment, the latter is much less well recognized. We have seen that T_s is the highest temperature at which the crystal can remain structurally stable. Since T_m is always lower than T_s , the region $T_m < T < T_s$ is the temperature range of superheating. It also follows that in this region the crystal is in a metastable state, or in other words, T_s is the upper limit of metastability, and in a sense the thermal analogue to the ideal strength of the crystal.

Despite the extensive efforts in studying the phenomenon of melting [36] certain aspects of this fundamental transition were not clarified until recently. One basic question that was raised [37] is the role of surfaces or interfaces in the mechanism of melting. From the standpoint of thermodynamics, melting occurs at the temperature at which the solid and liquid phases coexist, as expressed by the equality of the Gibbs free energies. However, thermodynamics says nothing about how melting occurs, or how long the process will take. These are issues pertaining to the kinetics of the phenomenon. Thus one can ask whether our thermodynamic picture of melting is one which is consistent with the kinetics [38]. This is a question that can be addressed by molecular dynamics simulation in that simulation provides a method to calculate the free energies of the solid and liquid phases [40, 41], as well as to directly observe the actual melting process at the molecular level [38, 42].

In any simulation study of melting it is essential to recognize that the melting point of the simulation model, T_m , can be quite different from the known melting point of the real substance. How well these two temperatures agree is, in fact, a useful indication of how realistic is the interatomic potential function on which the model is based. We will examine the question of the interplay between thermodynamics and kinetics in the particular case of a simulation model of silicon based on the empirical potential model developed by Stillinger and Weber [39]. For this potential free energy calculations have been reported by Broughton and Li [40] which gives the melting point T_m at 1691 ± 30 K. Given that the experimental melting point is 1683 K, the excellent agreement between 'theory' and experiment should be regarded as somewhat fortuitous.

Once T_m for the model is known, one then has the proper reference temperature from which to investigate the onset of melting. By taking a perfect crystal model of silicon, composed of 704 atoms in a cell with periodic boundary conditions, and heating it up to T_m using MD, it is found that over a reasonable period of simulation the system shows no indications of any onset of structural disordering. This apparent stability persists up to temperatures well beyond T_m ; it is only when T reaches 2500 K that the crystal is observed to suddenly undergo significant disordering over a period of 0.18 ps. These simulation results are perplexing at first sight. Why did the simulation model not melt at T_m as predicted by thermodynamics? Should the disordering at 2500, hereafter denoted as T_s be interpreted as the onset of melting?

To answer these and other questions, another set of simulations is performed using a simulation cell which has free surfaces in one direction, and periodic border in the other two directions. The important point to note is that we are now going to interpret the temperature of 2500 K when the crystal collapsed as the mechanical melting temperature T_s . Since the crystal cannot remain stable this point, there is no reason to do any simulation at temperatures above T_s . So the foregoing simulations are useful in arriving at this upper limit. We can therefore regard T_s as the 'theoretical strength' against thermal agitation (heating), just like the theoretical strength σ_c against mechanical deformation which we have discussed in Sec. 2.1.

The simulation runs in the case of a free surface are made in the temperature range above what we think should be the value of T_m as given by the free-energy calculation, but always below T_s . It is observed that structural disordering, which has all the features of local melting, begins invariably at the surface and then spreads toward the interior of the simulation cell. For a quantitative measure of the local disorder, we divide the cell into equal slices along the direction of the surface normal, and calculate the static structure factor $S(\underline{K})$ for each individual slice, with \underline{K} chosen to be a reciprocal lattice vector with orientation parallel to the surface. From the profile of $S(\underline{K})$ obtained at various intervals during the simulation, we can locate the melt-crystal interface, and by following this interface in time we determine its velocity of propagation $v(T)$ at a fixed temperature T . This procedure can be repeated for several temperatures to arrive at a temperature variation of the interfacial velocity. One can now ask what is the temperature at which the interface no longer moves.

As shown in in Fig. 7, the five data points in our particular study extrapolate to a temperature of 1710 K at zero interface velocity. The meaning of this extrapolation is simple but well worth appreciating. When the velocity of the melt-crystal vanishes, it clearly means that the two phases - the melt (liquid) on the defect side of the interface and the crystal on the bulk side - are 'in equilibrium' in the sense that neither side want to expand into the other, in other words, the two phases are 'in coexistence'. This then is the operational realization of the thermodynamic definition of crossing of the crystal and liquid free-energy curves. If this argument is valid, then one can expect the extrapolated temperature to be the temperature for thermodynamic melting. We note that 1710 is well within the uncertainties in the present study to the free-energy calculation value of 1691, which itself has uncertainties estimated to be 30K.

Similar studies of defect-induced melting also have been carried out using a bicrystal simulation cell representating a grain boundary, and another cell representing a crystal with voids of various sizes [38]. In both cases, extrapolation of the melt-crystal interface velocity leads to essentially the same value of T_m . The conclusion which one can draw from this series of simulations is that there exist in every material two types of melting, thermodynamic and mechanical.

(i) Thermodynamic melting at T_m requires a surface or other defect nucleation site for the formation of a liquid layer which then propagates into the crystalline bulk at a velocity which depends on the degree of superheating. This process is heterogeneous.

(ii) Mechanical melting at T_s ($> T_m$) is a homogeneous process; it is the upper limit of metastability.

As a final comment we note that recent studies also have been extended to grain boundaries where no premelting has been found although local disordering does take place at $T < T_m$ [43].

3.3 Solid-State Amorphization

When a homogenous, defect-free lattice is driven to structural instability by hydrostatic compression, two types of responses generally can be expected. The crystal can undergo a polymorphic transition to another lattice structure, or a transition to a disordered state, known as solid-state amorphization. Molecular dynamics simulations of compression loading on Si [19] and cubic SiC (β -phase) [22] using essentially the same many-body interatomic interaction model have shown that the former undergoes a transition from diamond cubic to β -Sn tetragonal structure, while the latter undergoes amorphization. The behavior of stability criteria in these two studies are shown in Fig. 8, where one sees that the two transitions involve different instability modes, the vanishing of the tetragonal shear modulus G' and the rhombohedral shear modulus G , respectively. The potential models from which the elastic constants are calculated are of the same bond-order form proposed by J. Tersoff for covalent crystals [24]. In both cases, the critical strains predicted in Fig. 8 agreed with what was observed in the direct simulations. The question then arises as to what is the underlying cause of the different structural consequences of shear instability.

It is apparent that an obvious difference between the two lattices is that one is an elemental system while the other is a binary (AB) compound. Thus in SiC there are chemical ordering effects which are not present in Si. Since in the context of chemical ordering a distinction is made between atomic size effects and chemical bonding effects, it is of interest to assess which effect is more responsible for the observed amorphization. For this analysis one can manipulate the description of interatomic interactions to *intentionally* suppress one effect or the other. Two modified forms of the Tersoff potential model have been produced, in one variant chemical bond preference is suppressed through an adjustment of the interaction between atoms of different species (model I), and in another variant size effects are suppressed by adjusting the bond-order parameter and cross interaction at the same time to leave heat of mixing unchanged (model II) [33]. The relevant physical properties of the Tersoff potential for β -SiC and its two modifications are shown in Table I. It is clearly seen that elimination of chemical bonding preference has little effect (model I), whereas all three elastic constants are significantly altered in the absence of atomic size difference. Although both $C_{11} - C_{12}$ and C_{44} are appreciably reduced, the lowering of the former is more drastic such that in model II the instability mode becomes the vanishing of G' . Thus one may deduce that not only is the presence of size effects responsible for the rhombohedral shear instability in β -SiC, but also their absence allows the tetragonal shear to vanish first in Si. To explicitly verify that these interpretations are correct, a simulation of model II under compression was carried out, indeed revealing a transition from zinc-blende to rock salt structure triggered by a tetragonal shear instability. This is an illustration of the use of modified or manipulated interatomic interaction in simulation; it can be a potentially very useful device for isolating cause-and-effect in probing complex phenomena.

We have demonstrated that in terms of the competition between instability modes, in this case the vanishing of the two shear moduli, one can gain some insight into the underlying nature of polymorphic and crystal to amorphous transitions. With regard to the experimental implications of our results on β -SiC, we note that amorphization of β -SiC single crystals induced by electron irradiation have been reported [44], the data revealing chemical disordering to take place below a critical temperature of 340 C. On the other hand, the structural transition in β -SiC under compression is found by X-ray diffraction to be polymorphic, from zinc-blende to a rock salt-type structure at 100 GPA [45]. The reason that the simulation predictions do not match precisely with the experimental findings can be attributed to two factors. First is that the empirical classical interatomic potential description is likely not adequate to correctly resolve competing mechanisms involving subtle effects of chemical bonding. Secondly, the role of crystal defects in

controlling the experimental observations has not been quantitatively assessed, while for the simulations one knows for sure that no defects were initially present. These uncertainties aside, it is noteworthy that both amorphization and polymorphic transitions have been observed in β -SiC. Apparently, under the relatively 'gentle' driving force of pressure the latter, associated with $G'=0$, prevails over the former which entails $G=0$. The driving force induced by electron irradiation is the destabilizing effect of point defect production; under this condition β -SiC undergoes amorphization rather than transforming to another crystal structure.

Even though in β -SiC pressure-induced amorphization appears to be precluded by a polymorphic transition, several experimental studies of this phenomenon in AB compounds can be cited to provide further insights into the kinetics of competing transitions. X-ray measurements show that Nb_2O_5 becomes amorphous at 19.2 GPa at 300 K which is novel because the oxide is simultaneously reduced in the process [46]; the competing polymorphic transition is believed to be kinetically impeded. In BAs a transformation from zinc blende to amorphous structure was observed at 125 GPa, just slightly above the calculated equilibrium transition pressure to the rock salt phase, and interpreted as signifying a kinetically frustrated process [47]. In more complicated systems, such as CaSiO_3 and MgSiO_3 perovskites, it has been conjectured that stress-induced amorphization arises from the near simultaneous accessibility of multiple modes of instability [48]. The amorphization of α -quartz (SiO_2) under pressure is a particularly well-known case where molecular dynamics simulation gives a transition pressure in agreement with experiment [49]. The physical mechanism underlying the elastic instability was first identified as the softening of a phonon mode [50]; later a dynamic instability associated with a soft phonon mode at one wave vector was found [51]. These developments are not surprising in view of our discussions in Section 2. It is interesting that the dynamic instability in α -quartz precede the elastic instability, occurring at 21.5 GPa and 25 GPa respectively.

4. Single Dislocation Dynamics

Dislocations, being the carriers of crystal plasticity, play a fundamental role in any consideration of lattice deformation [52]. For an overview of current atomistic and mesoscale studies of single and multiple dislocations, one may refer to a survey by Bulatov and Kubin.[53] Here we will discuss rather briefly two problems concerning single dislocation mobility to illustrate the kind of mechanistic issues of interest in this active area of simulation research. The first is an-going MD investigation of edge dislocation motion in a metal. This will show the information that direct atomistic simulation can provide. The second problem, an example of multiscale modeling, is the simulation of the dislocation velocity in a semiconductor using a kinetic Monte Carlo approach with kink activation energies determined by atomistic calculations.

4.1 MD simulations

We are presently conducting MD simulation of moving a pair of edge dislocations in a single crystal of bcc Mo by applying a shear stress [54]. The interatomic potential we use is an effective-medium approximation proposed by Finnis and Sinclair.[55] The set-up of the simulation cell and the application of stress are described in Fig. 9. Because of the use of periodic boundary conditions, the edge dislocation appears as a dipole. The geometry is such that the two dislocations are arranged to glide on the $\{112\}$ plane under an applied shear stress σ_{xy} . A method of comparing relative registry of atoms on two adjacent rows is used to locate the dislocation core during its glide. The dislocation profile,

shown in Fig. 10, suggests that while double kink nucleation is quite predominant, there is very little kink spreading or migration.

The stress and temperature dependence of the resulting dislocation velocity are shown in Figs. 11 and 12 respectively. In Fig. 11 the simulation results at 77K are seen to lie in the high-stress high-velocity region, while the experimental data are available only in the low-stress and low-velocity regime. The inset is a plot of the experimental dislocation velocity of KBr where a sharp increase of the velocity with increasing stress has been observed. Thus there is some basis for anticipating that the experimental curve for Mo will join onto the simulation results. The temperature dependence of the drag coefficient is shown in Fig. 12. From the increase of the drag coefficient with temperature one can conclude that the dislocation mobility is governed by the phonon drag mechanism.

4.2 Mesoscale Modeling

Covalent bonding in silicon and other semiconductors gives rise to a high barrier to dislocation motion [55]. To quantify this behavior in terms of the underlying atomistic mechanisms, much theoretical effort has been expended on obtaining accurate activation parameters for kink nucleation and migration. However, despite the recent progress and a considerable body of experimental observations, how dislocations actually move from one Peierls valley to another under stress is still an open question. The fundamental difficulty is that interpretation of the available data has been hampered by the lack of a theoretical description which is sufficiently free of ad hoc assumptions and capable of relating dislocation mobility behavior to the underlying kink mechanisms.

We consider here such a description by adopting a kinetic Monte Carlo treatment of kink nucleation, migration and annihilation processes along with full elastic interactions between the dissociated partial dislocations [56]. The formulation is designed to produce the overall dislocation movement as the cumulative effect of a large number of individual kink events, requiring for input only the kink formation and migration energies available from atomistic calculations [57]. Using this model we show that current atomistic data on activation energies give the velocities of a dissociated screw dislocation which bracket the experimental data; in the process we obtain bounds on the values of the activation energies to guide future studies. In focusing on the variation of dislocation velocity with applied stress, we show that the coupling between the two dissociated partials can be characterized in terms of compatibility between the strong Peierls barrier and the combined action of the stacking fault attraction and the elastic repulsion between dislocation segments which also influences the average separation distance between the partials X_0 .

We identify two compatibility scenarios of particular interest, when X_0 is an integral or half-integral multiples of the period of the Peierls barrier, and demonstrate that these two conditions give rise to distinct velocity variations with stress. When the average separation is commensurate with the period (integral X_0), the dislocation mobility is low at low stress and increases super-linearly below a critical stress value. In the case when X_0 is half-integral, no threshold behavior is observed and the velocity is essentially linear in the stress. Both types of variations have been observed experimentally. Previous attempts to rationalize the threshold behavior have resulted in the postulate of a random distribution of weak obstacles or "dragging points" on the dislocation line [58-60], a notion which we are able to clarify with the present description.

Our model deals with a screw dislocation with Burger's vector $(a/2)[1\bar{1}0]$ dissociated into two 30° partials in the (111) plane. Each partial is represented by a piecewise straight line composed of alternating horizontal (H) and vertical (V) segments. The length of H-segments can be any multiple of $a/2$, while the V-segments are all of the same

length, the kink height h . The stacking fault bounded by the two parallel partials has a width measured in multiples of h . The simulation cell is oriented with the partials running horizontally so that periodic boundary condition can be applied in this (z) direction. The dislocation glides in the vertical direction, upward being along $\langle 11\bar{2} \rangle$ (x), as a result of co-migration of the two partials which in turn follows from the elementary kink events.

In each simulation step, a stochastic sampling is carried out to determine which event will take place next: a kink pair nucleation on the H-segments in the upward (downward) direction or a kink (V-segment) translation to the left (right) by an amount b . The rates of these elementary events are calculated based on the energetics of the corresponding kink mechanisms. For example, for a kink pair nucleation mechanism three energy terms are considered, a formation energy obtained by relaxing the atomic configuration of the kink pair using an empirical potential or first principles methods, an energy bias which favors the reduction of the stacking-fault area, and the elastic interaction between a given segment and all the other segments and applied stress (so-called Peach-Koehler interaction). Accordingly, the nucleation rate for an embryonic double-kink (width one b) on a partial with Burgers vector \underline{b}_p and under stress σ_{ij} is calculated as

$$j_{kp} = \omega_o \exp\left(-\frac{E_k + (\pm\gamma_{SF} - \sigma:\underline{b}_p)A / 2}{k_B T}\right) \quad (14)$$

where ω_o is the pre-exponential "frequency" factor, which we set equal to the Debye frequency. γ_{SF} is the stacking fault energy, with '+' or '-' sign for the leading and trailing partials respectively. A is the area swept out by the dislocation during kink pair nucleation, with '\$+\$' or '\$-\$' sign for upward or downward nucleation respectively. The factor of 1/2 appears because we assume that in the saddle point configuration the dislocation has swept out half of the total area A . k_B is the Boltzmann's constant and T is the temperature. Similar expressions, with appropriate modifications, hold for the kink migration rates. The remaining barrier terms, such as E_k , are imported directly from atomistic simulation data.

We will rely on atomistic calculations to provide values for the kink formation and migration energies. Based on various calculated and experimental estimates available at present, a reasonable set of values to take for (E_k and W_m) would be around (0.7 eV, 1.2 eV). The dislocation velocity results obtained by using the kinetic Monte Carlo method just described are shown in Fig. 13 (solid line) along with two sets of experimental data (open symbols) [61,62]. In Fig. 13 we show the comparison of predicted stress dependence of the dislocation velocity at $T = 1000$ K, the open symbols, circles and diamonds, refer to the data of Imai and Sumino [62] and George [61] respectively, whereas the closed symbols denote the kinetic Monte Carlo simulations. One can see that depending on whether X_0 has integral or half integral value, the velocity varies smoothly (circle symbols) or shows a starting stress behavior (diamonds) [56].

5. Atomistics of Crack Propagation

A crystal is said to be intrinsically brittle if an existing crack is able to propagate along a crystallographic plane in a cleavage manner when the solid is under stress. If a material is intrinsically brittle, then it is capable of undergoing a transition to ductile behavior, emission of dislocations with crack-tip blunting, at a characteristic temperature T_{BD} . This transition has been and continues to be a formidable challenge to our theoretical understanding of fracture mechanics. In this section we will describe two atomistic

simulation studies of crack-tip extension, first a demonstration that brittle-ductile transition can be observed in a dynamical scenario, then followed by a characterization of dislocation emission in the stress field at a crack tip.

5.1 Brittle-Ductile Transition

Before discussing the simulation of brittle-to-ductile transition we consider first the set up of the simulation cell containing a crack tip. Fig. 14 shows a schematic of a macroscopic elastic body containing an atomically sharp crack of length $2c$ subject to an uniaxial tensile loading σ . If we focus on a small region containing one of the crack tips, then we have a simulation cell composed of N atoms (N is around 4000 in the study we will discuss). It is understood that the cell is large enough that the region beyond the cell border can be reasonably well treated as an elastic continuum. Thus we can throw away the elastic medium beyond the border and represent the effects of this medium on the interior atoms by a traction imposed at the cell border [63]. For the third direction, that coming out of the plane of the paper, we will use periodic boundary condition, so the problem is one of plane strain. To demonstrate that this treatment of the border condition does not introduce appreciable numerical artifact, we first study the simpler problem of determining the critical stress for cleavage fracture.

It is well known in fracture mechanics that the Griffith criterion provides a good overall estimate of this critical stress. In the case of an anisotropic lattice the criterion takes the form [64],

$$K_{IG} = \sqrt{2\gamma} \{ (s_{11}s_{22} / 2)^{1/2} [(s_{22} / s_{11})^{1/2} + (2s_{12} + s_{66}) / 2s_{11}]^{1/2} \}^{-1/2} \quad (15)$$

where K_{IG} denotes the critical value of the stress intensity factor for pure tensile loading (mode I), s_{ij} are the compliance constants with indices 1, 2, and 6 referring to the directions of plane strain, crack propagation (normal to crack front), and normal of the crack plane, respectively. In essence this result is a consequence of imposing the equilibrium condition between strain-energy release rate and twice the surface energy of the crack surface [65]. The Griffith condition has been tested in a number of simulation studies on crack propagation, with varying results. We have shown that it is satisfied to within about 5% for three different crack-tip configurations [66]. This is a significant improvement over previous studies which found deviations from the Griffith condition ranging from 20% to a factor of 3; it is achieved through a combination of better treatment of border conditions, taking into account crystal anisotropy, and more careful handling of the numerical data.

Fig. 14 shows the MD simulation results on $\alpha - Fe$, obtained using an Embedded-Atom-Method potential, . On the left hand side one sees the development of a crack tip under mode I loading at 10% above the Griffith critical value K_{IC} after simulation at the indicated temperature for 3000 time steps. Except for the different temperatures, all three simulations are identical. In the simulation at $T = 300$ K the crack has advanced in a cleavage manner (crack tip position at $t = 0$ is indicated by the cross) with a smooth crack surface profile. The middle result at $T = 400$ K is quite different; here one sees a significant deformation in the upper part of the crack surface. This is a signature of plastic deformation or dislocation emission. At $T = 500$ K the deformation at the crack tip is so severely that the crack has blunted and is opening up rather than moving forward (to the right). These results constitute the direct observation of a crack tip undergoing a brittle-to-ductile transition [67]. The right hand side of Fig. 14 shows what happens if one continues the simulation at $T = 500$ K out to longer times. One sees that at time step 5000 a step appears in the upper border of the simulation cell. This step is created by the movement of a dislocation from the crack tip up to the border.

5.2 Crack Tip Plasticity

In the context of understanding materials strength from a multiscale point of view, crack-tip plasticity is a problem that can benefit significantly from the linking of different simulation techniques [68,69]. A central issue that should be resolved at the atomistic level is under what condition a dislocation will be emitted at the crack tip; this is a process that can be realistically captured by MD simulation. At the microstructure level, questions concerning the distribution of dislocations in the plastic zone ahead of the crack tip and their shielding effects on crack extension are particularly relevant. These problems are more properly treated by mesoscale simulation techniques such as discrete dislocation dynamics (DDD) and finite-element method (FEM).

The process of dislocation nucleation at a crack tip is a fundamental problem in the mechanical behavior of stressed crystalline solids at finite temperatures, particularly in the context of understanding the brittle-to-ductile transition [70,71]. Because the crack-tip region is inherently nonlinear and extends over essentially molecular dimensions, the problem would appear to be ideally suited for atomistic simulation [66,67]. From the standpoint of continuum analysis, criteria for predicting brittle or ductile behavior [71,72] are usually based on the concept of the energy-release rate (actually an energy per unit area) for cleavage decohesion, G_{cleav} , and dislocation nucleation, G_{disl} . A ductile material is then characterized by $G_{\text{disl}} < G_{\text{cleav}}$, where $G_{\text{cleav}} = 2\gamma$, the energy of the two crack surfaces [65]. Recent progress has been achieved by introducing an interplanar potential associated with rigid block sliding in a homogeneous lattice [71]. Using heuristic models for this potential, which is equivalent to specify the stress-displacement constitutive relation on the slip plane, the critical configurations for dislocation nucleation from the crack tip can be calculated, and in this manner estimates of the brittle-to-ductile transition temperature can be made [73,74].

In a 3D MD simulation of a microcrack in an fcc lattice under tensile loading (plain strain mode I) using the Lennard-Jones potential, the process of dislocation emission from a crack tip has been isolated, and an appropriate stress-displacement relation extracted from the atomic-level displacement and stress fields [75]. The geometric setup, with (221) being the crack plane, is shown at the top of Fig. 15. The simulation cell dimensions are $3a$, $60a$, and $120a$ in the x -, y -, and z -directions respectively (86,400 atoms), with lattice parameter $a = 1.56\sigma$, σ being the length parameter in the potential. Periodic conditions are imposed in the x - and y -directions, while surface traction is applied on the z -borders. Simulations are carried out at very low temperatures.

In the lower left part of Fig. 15 we show an instantaneous atomic configuration during simulation in which one can see that the crack tips have not advanced from their initial positions (shaded region), while two stacking faults on the (111) planes at $\theta = 54.7^\circ$ have propagated into the bulk. At one end these stacking-fault strips are bounded by a moving partial dislocation, with Burgers vector $b = [112]/6$ and $\phi = 0^\circ$; at the other end they are bounded by a step on the (221) crack surface. This result demonstrates that MD simulation is able to capture the dynamic process of dislocation *emission*, including the *nucleation* from the crack tip and the *motion* away from the crack.

The atomistic results that are most relevant to continuum model formulation are not the atomic positions given by the simulation, rather they are the shear and opening displacements, δ_r and δ_θ , which are components obtained by decomposing the atomic-level displacement field along the slip plane, as indicated in the lower inset in Fig. 15. In the lower right part of the figure we show the variations of displacements δ_r with position

r (see the schematic at the top) at various durations of simulation. At any given simulation time during slip along the (111) plane, δ_r decreases monotonically with increasing r; this is to be expected since shear displacement should be the largest just in front of the crack tip. As time increases, all the displacements are seen to increase; however, once δ_r reaches a value of b, the dislocation core has moved past that particular atomic site, therefore no further displacement occurs at that site.

Knowledge of the instantaneous atomic positions allows one to calculate the internal stress field, either from its mechanical definition of force across a plane which is a tedious task, or from the virial expression for the atomic-level stress [76]. While the latter method is considerably simpler, its validity in the immediate vicinity of a structural inhomogeneity is open to question. Once the stress field is determined, it can be resolved into shear and tensile components, τ and σ , on the slip plane. With the resolved displacement and stress components in hand, one can cross plot and thus generate shear and tensile stress-displacement curves, $\tau(\delta_r)$ and $\sigma(\delta_\theta)$. Various $\tau(\delta_r)$ results obtained at different distances between the crack tip and the dislocation are shown in Fig. 15.

In contrast to the present direct determination of the shear stress-displacement relation, one can assume a certain form for $\tau(\delta_r)$ and fit the parameters to any known property. As a simple approximation Rice proposed to take for $\tau(\delta_r)$ the Frenkel-Peierls sinusoid, and moreover, identified its integrated area between $\delta_r=0$ and the first zero of $\tau(\delta_r)$ with a quantity γ_{us} , which he called the "unstable-stacking-fault energy", given by the maximum energy encountered during the rigid-block like sliding along the slip plane of one half of a perfect crystal relative to the other [71]. This approximation implies that the actual nonuniform displacement field on the slip plane in the presence of a nucleating dislocation may be replaced by a uniform displacement distribution corresponding to the rigid-block sliding. For further discussions of using the results of Fig. 15 to examine the validity of the approximation, the interested reader should see ref [75].

6. An Outlook on Multiscale Materials Modeling

Multiscale materials modeling has emerged as a significant concept in computational materials research. We examine several case studies which seek to provide understanding of mechanical behavior of solids at the atomistic level, in the context of upper and lower limits to strength and deformation, the interplay between melting and stability criteria, the competition between pressure-induced polymorphism and amorphization, the role of kink mechanism in dislocation mobility, and the concept of a local free energy as an invariant measure of defect driving force. Through these illustrations we express the optimistic belief that further pursuits of this kind would be worthwhile.

References

- [1] Report of the National Workshop on Advanced Scientific Computing, July 30-31, 1998 (National Academy of Sciences), available from <http://www.er.doe.gov/production/octr/mics/index.html>
- [2] Special Issue of J. Computer-Aided Mater. Design, vol. 3, (1996); special issue of Current Opinion in Solid State and Mater. Sci., vol. 3, no. 6 (1998).
- [3] G. H. Campbell et al., Mater. Sci. Eng. **A251**, 1 (1998).
- [4] M. Born, Cambridge Philos. Soc. **36**, 160 (1940).

- [5] M. Born and K. Huang, *Dynamical theory of Crystal Lattices* (Clarendon, Oxford, 1956).
- [6] R. Hill, Math. Proc. Camb. Phil. Soc. **77**, 225 (1975).
- [7] R. Hill and F. Milstein, Phys. Rev. B **15**, 3087 (1977).
- [8] A. Kelly and N. H. Macmillan, *Strong Solids* (Clarendon, Oxford, 1986), 3rd ed..
- [9] J. Wang, J. Li, S. Yip, S. Phillpot, D. Wolf, Phys. Rev. B **52**, 12627 (1995).
- [10] Z. Zhou and B. Joos, Phys. Rev. B **54**, 3841 (1996)..
- [11] J. W. Morris and C. R. Krenn, Philos Mag. A **80**, 2827 (2000).
- [12] J. W. Gibbs, in *The Scientific Papers of J. Willard Gibbs, Vol. 1: Thermodynamics* (Ox Bow Press, Woodbridge, Conn. 1993), p. 55.
- [13] J. W. Morris et al.
- [14] D. C. Wallace, *Thermodynamics of Crystals*, Wiley, New York (1972).
- [15] T. H. K. Barrons and M. L. Klein, Proc. Phys. Soc **85**, 523 (1965).
- [16] W. G. Hoover, A. C. Holt, D. R. Squire, Physica **44**, 437 (1969).
- [17] Basinski ??.. cited in Zhou and Joos [11] --- LJ attention !!
- [18] J. Wang, S. Yip, S. Phillpot, D. Wolf, Phys. Rev. Lett. **71**, 4182 (1993).
- [19] K. Mizushima, S. Yip, E. Kaxiras, Phys. Rev. B **50**, 14952 (1994).
- [20] M. Tang and S. Yip, J. Appl. Phys. **76**, 2716 (1994).
- [21] F. Cleri, J. Wang, S. Yip, J. Appl. Phys. **77**, 1449 (1995).
- [22] M. Tang and S. Yip, Phys. Rev. Lett. **75**, 2738 (1995).
- [23] J. Tersoff, Phys. Rev. B **39**, 5566 (1989).
- [24] J. Li, Ph.D. Thesis, MIT (2000).
- [25] G. Galli, F. Gygi, A. Catellani, Phys. Rev. Lett. **82**, 3476 (1999).
- [26] M. Born, J. Chem. Phys. **7**, 591 (1939).
- [27] L. Hunter and S. Siegel, Phys. Rev. **61**, 84 (1942).
- [28] S. M. Foiles, M. I. Baskes, M. S. Daw, Phys. Rev. B **33**, 7983 (1986).
- [29] M. Parrinello and A. Rahman, J. Appl. Phys. **52**, 7182 (1981).
- [30] J. R. Ray, Comput. Phys. Rept. **8**, 109 (1988).
- [31] J. Wang, J. Li, S. Yip, D. Wolf, S. Phillpot, Physica A **240**, 396 (1997).
- [32] L. L. Boyer, Phase Transitions **5**, 1 (1985).
- [33] J. F. Lutsko, D. Wolf, S. R. Phillpot, S. Yip, Phys. Rev. B **40**, 2841 (1989).
- [34] D. Wolf, P. R. Okamoto, S. Yip, J. F. Lutsko, M. Kluge, J. Mater. Res. **5**, 286.
- [35] J. L. Tallon, Nature (London) **342**, 658 (1989).
- [36] A. R. Ubbelohde, *Molten States of Matter: Melting and Crystal Structure* (Wiley, Chichester, 1978).
- [37] R. W. Cahn, Nature **323**, 668 (1986).
- [38] S. R. Phillpot, J. F. Lutsko, D. Wolf, S. Yip, Phys. Rev. B **40**, 2831 (1980); S. R. Phillpot, S., D. Wolf, Computers In Physics **3**, no. 20, p. 20 (1989).
- [39] F. H. Stillinger and T. A. Weber, Phys. Rev. B **31**, 5262 (1985).
- [40] J. Q. Broughton and X. P. Li, Phys. Rev. B **35**, 9120 (1987).
- [41] M. de Koning, A. Antonelli, S. Yip, Phys. Rev. Lett. **83**, 3473 (2000); J. Chem. Phys., submitted.
- [42] J. Solca, A. J. Dyson, G. Steinbrunner, B. Kirchner, H. Huber, Chem. Phys. **224**, 253 (1997).
- [43] T. Nguyen, S. Yip, P. S. Ho, T. Kwok, C. Nitta, Phys. Rev. B **46**, 6050 (1992).
- [44] H. Inui, H. Mori, A. Suzuki, H. Fujita, Philos. Mag. B **65** (1992) 1.
- [45] M. Yoshida, A. Onodera, M. Ueno, K. Takemura, O. Shimomura, Phys. Rev. B **48** (1993) 10587.
- [46] G. C. Serghiou, R. R. Winters, W. S. Hammack, Phys. Rev. Lett. **68** (1992) 331.
- [47] R. G. Greene, H. Luo, A. L. Ruoff, Phys. Rev. Lett. **73** (1994) 2476.
- [48] M. Hemmati, A. Chizmeshya, G. H. Wolf, P. H. Poole, J. Shao, C. A. Angell, Phys. Rev. B **51** (1995), 14841.

- [49] J. S. Tse and D. D. Klug, Phys. Rev. Lett. **67** (1991) 3559.
- [50] N. Binggeli, N. R. Keskar, J. R. Chelikowsky, Phys. Rev. B **49** (1994) 3075.
- [51] G. W. Watson and S. C. Parker, Phys. Rev. B **52** (1995), 13306.
- [52] Hirth and Lothe
- [53] Bulatov and Kubin
- [54] J. P. Chang, HK Symp
- [55] M. S. Duesbery and G. Y. Richardson, Crit. Rev. Solid State **17**, 1 (1991).
- [56] W. Cai, V. V. Bulatov, J. F. Justo, A. S. Argon, S. Yip, Phys. Rev. Lett. **84**, 3346 (2000)
- [57] V. V. Bulatov, S. Yip, A. S. Argon, Philos. Mag. A **72**, 453 (1995).
- [58] V. Celli, M. Kabler, T. Ninomiya, R. Thomson, Phys. Rev. **131**, 58 (1963).
- [59] H. J. Möller, Acta Metall. **26**, 963 (1978)).
- [60] H. Alexander, in *Dislocations in Solids*, F. R. N. Nabarro ed. (North Holland, Amsterdam, 1986), vol. 7, p. 113.
- [61] A. George, J. Phys. (Paris) **40**, 133 (1979).
- [62] M. Imai and K. Sumino, Philos. Mag A **47**, 599 (1983).
- [63] B. deCelis, A. S. Argon, S. Yip, J. Appl. Phys. **54**, 4864 (1983)
- [64] G. C. Sih, G. C. and H. Liebowitz, in *Fracture: An Advanced Treatise*, H. Liebowitz, ed. (Academic, New York, 1968), vol. 2, p. 67.
- [65] A. A. Griffith, Philos. Trans. Roy. Soc. A **221**, 163 (1920).
- [66] K. S. Cheung, S. Yip, Phys. Rev. Lett. **65**, 2804 (1990).
- [67] K. S. Cheung and S. Yip, Modell. Simul. Mater. Sci. Eng. **2**, 865 (1994).
- [68] E. Kaxiras and S. Yip, Current Opinion in Solid State & Mater. Sci. **3**, 523 (1998).
- [69] F. E. Abraham, J. Q. Broughton, N. Bernstein, E. Kaxiras, Computers In Phys. **12**, 538 (1998).
- [70] A. S. Argon, Acta metall. **35**, 185 (1987).
- [71] J. R. Rice, J. Mech. Phys. Solids **40**, 239 (1992).
- [72] J. R. Rice and R. Thomson, Phil. Mag. **29**, 73 (1974).
- [73] A. S. Argon, G. Xu, M. Ortiz, Mat. Res. Soc. Symp. Proc. **409**, 29 (1996).
- [74] G. Xu, A. S. Argon, M. Ortiz, Phil. Mag. A **75**, 341 (1997).
- [75] F. Cleri, S. Yip, D. Wolf, S. R. Phillpot, Phys. Rev. Lett. **79**, 1309 (1997).
- [76] K. S. Cheung, and S. Yip, J. Appl. Phys. **70**, 5688 (1991).